All Sciences Proceedings
http://as-proceeding.com/

1st International Conference on Scientific and Innovative Studies
April 18-20, 2023 : Konya, Turkey

https://as-proceeding.com/index.php/icsis

Buckling analysis of nanocomposite beams based on refined beam theory by considering the Agglomeration effect of CNTs

Ihab Eddine Houalef*, Ismail Bensaid [2] and Ahmed Saimi [3]

[1]*Mechanical engineering Department, Faculty of Technology, IS2M Laboratory, University of Abou Beckr Belkaid (UABT), Tlemcen, Algeria**
[2]*Mechanical engineering Department, University of Abou Beckr Belkaid (UABT), Tlemcen, Algeria*
[3]*Mechanical engineering Department, Faculty of Technology, IS2M Laboratory, University of Abou Beckr Belkaid (UABT), Tlemcen, Algeria*

(ihabihabeddine1@gmail.com)

Abstract – The present work deals with buckling load behavior of nanocomposite beams by considering the agglomeration effect of single-walled carbon nanotubes (CNTs) and different patterns CNTs in polymeric matrix. The material properties of nanocomposite beams are estimated using the Eshelby–Mori–Tanaka approach based on an equivalent fiber. The equations of motion are derived based on refined beam strain gradient theory, employing Hamilton's principle and using Differential Quadrature Finite Element Method (DQFEM) derived from the differential quadrature method (DQM). The results are compared with analytical results in the literature. It is remarked that mechanical properties and therefore critical buckling loads of nanocomposite beam are seriously affected by CNTs agglomeration.

Keywords – DQFEM, Buckling, Cnts, Agglomeration Effect Of CNT, Refined Higher-Order Beam Theory.

I. Introduction

Carbon nanotubes (CNTs) have been accepted as an excellent candidate for the reinforcement of polymer composites due to their high elastic modulus, tensile strength and low density.

Assessing the material properties of a CNTRC is of utmost importance, however using the traditional homogenization schemes for particle-reinforced composites might lead to an over estimation of the material properties, since CNTs tend to bundle together forming inclusions within polymeric matrices, which affects the mechanical properties of the resulting CNTRC, usually in a non-desirable manner. This phenomenon occurs due to their high aspect ratio, van der Waals forces and their low bending stiffness values. Wan et al. [1] investigated the effective moduli of the CNT-reinforced polymer composite with emphasis on the influence of CNT length and CNT matrix interphase on the stiffening of the composite. Some contributions have been provided to investigate the benefits of using aligned CNT reinforced polymer composites ([2], [3], [4], [5], [6], [7], [8], [9], [10]–[11]) determined the elastic properties of CNTRCs using a finite element investigation.

Wuite and Adali [12] found that the stiffness of CNTRC beams can be improved significantly by the homogeneous dispersion of a small percentage of CNTs. Vodenitcharova and Zhang [13] investigated the pure bending and bending-induced local buckling of CNTRC beams. However, the experimental and numerical studies concerning CNTRCs have shown that distributing CNTs uniformly as the reinforcements in the matrix can only achieve moderate improvement of the mechanical properties ([14]–[15]). This is mainly due to the weak interface between the CNTs and the matrix where a significant material property mismatch exists.

There are a few studies on the mechanical behavior of the CNTRC beams in the open literature. For example, Yas and Samadi [16] proposed free

vibration and buckling of FG-CNTR beams reinforced by aligned CNTs employing rule of mixture (ROM) and generalized differential quadrature (GDQ) method. Their results indicated that suitable distribution for CNTs could improve the free vibration and buckling characteristics of the CNTRC beams. Based on Reissner's mixed variational theorem and using ROM model, Wu and Chang [17] developed a unified formulation of finite layer methods for the three-dimensional buckling analysis of simply supported FG-CNTR plates with surface-bonded piezoelectric actuator and sensor layers and under biaxial compressive loads. They compared the buckling characteristics of three different types of CNTs distribution that were uniformly distributed (UD), FG rhombus, and X-type variations through the thickness coordinate.

Kolahchi et al. [18] studied the dynamic response of cylindrical shells submerged in an incompressible fluid subjected to earthquake, thermal, and moisture loads. Several parametric studies were carried out accounting the influences of the fluid, boundary condition, thermal load, moisture changes, structural damping parameter, length to thickness aspect ratio, CNTs volume fraction, and agglomeration state on the dynamic deflections of the structure. The results revealed that when considering the agglomeration effect the deflections increased. Recently, Tornabene et al. [19] investigated recovery of through-the-thickness transverse normal and shear strains and stresses in statically deformed FG doubly curved sandwich shell structures and shells of revolution using the generalized zigzag displacement field and the Carrera Unified Formulation.

In the present study, the buckling of the CNTRC beams is investigated using the DQFEM method. The Mori–Tanaka approach is employed to calculate the effective elastic moduli of the beam. New solutions of buckling loads based on refined beam strain gradient theory are presented and discussed in details. Different parameters effect, which have considerable impact on the numerical solutions, are also investigated.

II. Materials and Method

This section is divided in two main sub-sections, a first one where the two-parameter agglomeration model using the Eshelby–Mori–Tanaka approach is used for properties' prediction purpose and the second one devoted to the model development based on a refined beam strain gradient theory.

A. Properties of the equivalent fiber

The equivalent fiber for SWCNT with chiral index of (10, 10) is a solid cylinder with diameter of 1.424 nm. ROM is used inversely for calculating material properties of equivalent fiber are listed in Table 1. [20]

$$E_{11} = \eta_1 V_{cnt} E_{11}^{cnt} + V_p E^p \quad (1a)$$

$$\frac{\eta_2}{E_{22}} = \frac{V_{cnt}}{E_{22}^{cnt}} + \frac{V_p}{E^p} \quad (1b)$$

$$\frac{\eta_3}{G_{12}} = \frac{V_{cnt}}{G_{12}^{cnt}} + \frac{V_p}{G^p} \quad (1c)$$

where E_{LEF}, E_{TEF}, G_{EF}, ϑ_{EF}, E_{LC}, E_{TC}, G_C, ν_C, E_M, G_M, ν_M, V_{EF}, and V_M are respectively longitudinal modulus of equivalent fiber, transverse modulus of equivalent fiber, shear modulus of equivalent fiber, Poisson's ratio of equivalent fiber, longitudinal modulus of composites, transverse modulus of composites, shear modulus of composites, Poisson's ratio of composites, modulus of matrix, shear modulus of matrix, Poisson's ratio of matrix, volume fraction of the equivalent fiber, and volume fraction of the matrix. E_{LC},G_C and E_{TC} are obtained from multiscale FEM or molecular dynamics (MD) simulations, respectively.

Table 1. Material properties of equivalent fiber and matrix

Mechanical properties	Equivalent fiber	Matrix phase
Young's modulus	_	2.1
Longitudinal Young's modulus (GPa)	649.12	_
Transverse Young's modulus (GPa)	11.27	_
Longitudinal shear modulus (GPa)	5.13	_
Poisson's ratio	0.284	0.34
Density (kg/m3)	1400	1150

The agglomeration model based on the Eshelby–Mori–Tanaka homogenization scheme considers that the CNTs are randomly dispersed along the matrix, but some of them are known to be bundled together forming clusters. Those clusters or inclusions are modelled according to the Eshelby inclusion model, considering these inclusions will assume a spherical shape [21], as schematically represented in Figure 1.

The total volume of CNT reinforcement in the representative volume element (RVE) is denoted by V_r and is divided in $V_r^{cluster}$, which is the volume of CNTs inside a cluster, and V_r^m, which is the volume of CNTs dispersed in the matrix and the outside the clusters. Note that from now on, the subscripts r and m will stand for the reinforcing phase and for the matrix, respectively, thus one can express the total CNT volume fraction in the RVE according to

$$V_r = V_r^{cluster} + V_r^m \tag{2}$$

The two parameters used to describe the agglomeration are defined as

$$\mu = \frac{V_{cluster}}{V}, \quad \eta = \frac{V_r^{cluster}}{V_r} \quad 0 \le \eta, \mu \le 1 \tag{3}$$

Where V is the volume of RVE, $V_{cluster}$ is the volume of clusters in the RVE. μ is the volume fraction of clusters with respect to the total volume of the RVE and η is the volume ratio of the CNTs inside the clusters over the total CNT inside the RVE.

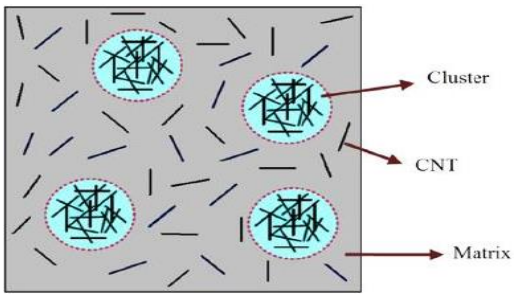

Fig. 1 Representation of the Eshelby inclusion model with spherical CNTs spherical inclusion

The effective bulk modulus K_{in} and shear modulus G_{in} of the cluster and the effective bulk modulus K_{out} and shear modulus G_{out} of the equivalent matrix outside the cluster can be calculated as [22]

$$K_{in} = K_m + \frac{f_r \eta(\delta_r - 3K_m\alpha_r)}{3\left(\mu - f_r\eta + f_r\eta\alpha_r\right)} \tag{4}$$

$$K_{out} = K_m + \frac{f_r(1-\eta)(\delta_r - 3K_m\alpha_r)}{3[1-\mu-f_r(1-\eta)+f_r(1-\eta)\alpha_r]} \tag{5}$$

$$\frac{\eta_3}{G_{12}} = \frac{V_{cnt}}{G_{12}^{cnt}} + \frac{V_p}{G^p} \tag{6}$$

$$G_{out} = G_m + \frac{f_r(1-\eta)(\eta_r - 2G_m\beta_r)}{2[1-\mu-f_r(1-\eta)+f_r(1-\eta)\beta_r]} \tag{7}$$

In equations (5)–(7), the mechanical terms $\alpha_r, \beta_r, \delta_r$ and η_r can be formulated in the following form

$$\alpha_r = \frac{3(K_m + G_m) + K_r - l_r}{3(G_m + K_r)} \tag{8}$$

$$\beta_r = \frac{1}{5}\left\{\frac{4G_m+2K_r+l_r}{3(G_m+K_r)} + \frac{4G_m}{G_m+P_r} + \frac{2[G_m(3K_m+G_m)+m_r(3K_m+7G_m)]}{G_m(3K_m+G_m)+m_r(3K_m+7G_m)}\right\} \tag{9}$$

$$\delta_r = \frac{1}{3}\left[n_r + 2l_r + \frac{(2K_r+l_r)(3K_m+2G_m-l_r)}{G_m+K_r}\right] \tag{10}$$

$$\eta_r = \frac{1}{5}\left[\frac{2}{3}\left(2\eta_r - l_r\right) + \frac{8G_m p_r}{G_m+p_r} + \frac{8m_r G_m(3K_m+4G_m)}{3K_m(m_r+G_m)+G_m(7m_r+G_m)} + \frac{2(K_r-l_r)(2G_m+l_r)}{3(G_m+K_r)}\right] \tag{11}$$

The subscripts m and r stand for the quantities of the matrix and the reinforcing phase, Km and Gm are the bulk and shear moduli of the matrix, respectively, and k_r, l_r, m_r, n_r, and p_r are the Hill's elastic moduli for the reinforcing phase (CNTs), which can be found from the equality of two following matrices

$$C_r = \begin{bmatrix} n_r & l_r & l_r & 0 & 0 & 0 \\ l_r & k_r+m_r & k_r-m_r & 0 & 0 & 0 \\ l_r & k_r-m_r & k_r+m_r & 0 & 0 & 0 \\ 0 & 0 & 0 & p_r & 0 & 0 \\ 0 & 0 & 0 & 0 & m_r & 0 \\ 0 & 0 & 0 & 0 & 0 & p_r \end{bmatrix} \tag{12}$$

$$C_r = \begin{bmatrix} \frac{1}{E_L} & -\frac{\nu_{TL}}{E_T} & -\frac{\nu_{ZL}}{E_Z} & 0 & 0 & 0 \\ -\frac{\nu_{LT}}{E_L} & \frac{1}{E_T} & -\frac{\nu_{ZT}}{E_Z} & 0 & 0 & 0 \\ -\frac{\nu_{LZ}}{E_L} & -\frac{\nu_{TZ}}{E_T} & \frac{1}{E_Z} & 0 & 0 & 0 \\ 0 & 0 & 0 & \frac{1}{G_{TZ}} & 0 & 0 \\ 0 & 0 & 0 & 0 & \frac{1}{G_{ZL}} & 0 \\ 0 & 0 & 0 & 0 & 0 & \frac{1}{G_{LT}} \end{bmatrix}^{-1} \tag{13}$$

where $E_L, E_T, E_Z, G_{TZ}, G_{ZL}, G_{LT}, \nu_{LT}$ are material properties of the equivalent fiber, which can be determined from the inverse of the ROM. It must be noticed that before the use of the ROM, material properties of nanoscale RVE of nanocomposite must be obtained from multiscale FEM analysis or MD simulations.

The effective bulk modulus K and the effective shear modulus G of the composite can be determined using the following expressions:

$$K = K_{out}\left[1 + \frac{\mu\left(\frac{K_{in}}{K_{out}} - 1\right)}{1 + \alpha(1-\mu)\left(\frac{K_{in}}{K_{out}} - 1\right)}\right] \tag{14}$$

$$G = G_{out}\left[1 + \frac{\mu\left(\frac{G_{in}}{G_{out}} - 1\right)}{1 + \beta(1-\mu)\left(\frac{G_{in}}{G_{out}} - 1\right)}\right] \quad (15)$$

in which

$$\nu_{out} = \frac{(3K_{out} - 2G_{out})}{2(3K_{out} + G_{out})} \quad (16)$$

$$\alpha = \frac{(1 + \nu_{out})}{3(1 - \nu_{out})} \quad (17)$$

$$\beta = \frac{2(4 - 5\nu_{out})}{15(1 - \nu_{out})} \quad (18)$$

Finally, the effective Young's modulus E and Poisson's ratio ν of the CNTRC are given according to

$$E = \frac{9KG}{3K + G} \quad (19)$$

$$\nu = \frac{3K - 2G}{6K + 2G} \quad (20)$$

Consider a straight CNTRC beam with length L and rectangular cross section $b \times h$, with b being the width and h being the height. The beam is made of polymeric matrix reinforced with single walled CNT (SWCNT), as shown in Fig. 2a. In this study, the beams are assumed to have four different patterns of reinforcement over the cross sections as shown in Fig. 2b. The functions that model the considered distributions are presented in the Table 2, where UD stands for uniformly distributed and FG stands for functionally graded.

Table 2. CNTs volume fraction distributions considered

CNTs Distributions	
UD-Beam	$f_r = f_r^*$
O-Beam	$f_r = 2\left(1 - 2\frac{\lvert z\rvert}{h}\right) f_r^*$
X-Beam	$f_r = 4\frac{\lvert z\rvert}{h} f_r^*$
V-Beam	$f_r = \left(1 + 2\frac{z}{h}\right) f_r^*$

The coordinate in the thickness direction varies within the interval $\left[-\frac{h}{2}, \frac{h}{2}\right]$, where h is the thickness of the beam and f_r^* is expressed by

$$f_r^* = \frac{W_r}{W_r + (\rho_r/\rho_m)(1 - W_r)} \quad (21)$$

where W_r is the mass fraction of CNTs.

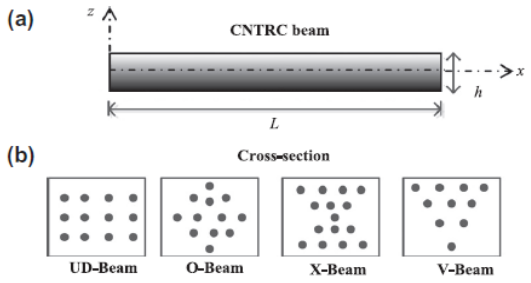

Fig. 2 Geometry of a CNTRC beam (a); and cross sections of different patterns of reinforcement (b)

B. *Formulation and theories*

B.1 Refined parabolic beam theory

In this section, refined parabolic beam theory is introduced in order to derive the kinematic relations of the beam. The displacement fields of the beam can be presented as follows

$$u(x,z,t) = u_0(x,t) - z\frac{dw_b}{dx} - f(z)\frac{dw_s}{dx} \quad (22)$$
$$w(x,z,t) = w_b(x,t) + w_s(x,t)$$

Where $u_0(x,t)$,$w_b(x,t)$ and $w_s(x,t)$ are, respectively, the in-plane displacement in x-directions, bending and shear components of the transverse displacement of points on the neutral axis of the beam; and $f(z)$ is a shape function. The nonzero strains of the beam can be written as

$$\varepsilon_{xx} = \frac{du_0}{dx} - z\frac{d^2w_b}{dx^2} - f(z)\frac{d^2w_s}{dx^2}, \quad (23)$$
$$\gamma_{xz} = g(z)\frac{dw_s}{dx}$$

where

$$g(z) = 1 - \frac{df(z)}{dz} \quad (24)$$

Using the linear elastic constitutive law, the normal stress σ_x and shear stress τ_{xz} are given by

$$\sigma_x(z) = Q_{11}(z)\,\varepsilon_x \quad (25)$$
$$\tau_{xz}(z) = Q_{55}(z)\,\gamma_{xz}$$

In which

$$Q_{11}(z) = \frac{E(z)}{1 - \nu^2}, \qquad Q_{55}(z) = \frac{E(z)}{2(1 + \nu)} \quad (26)$$

The element strain energy resulted from the foundation deformation is of the form

$$U_e^B = \frac{1}{2}\int_{V_e} \begin{Bmatrix}\sigma_x \\ \tau_{xz}\end{Bmatrix}^T \begin{Bmatrix}\varepsilon_x \\ \gamma_{xz}\end{Bmatrix} dV \quad (27)$$

$$U_e{}^B = \frac{1}{2} b \int_0^l \left[\left(I_1\frac{d^2u_0}{dx^2} + 2I_2\frac{du_0}{dx}\frac{d^2w_b}{dx^2} + 2I_3\frac{du_0}{dx}\frac{d^2w_s}{dx^2} + 2I_4\frac{d^2w_b}{dx^2}\frac{d^2w_s}{dx^2} + I_5\frac{d^2w_b}{dx^2}\frac{d^2w_b}{dx^2} + I_6\frac{d^2w_s}{dx^2}\frac{d^2w_s}{dx^2} + I_7\frac{dw_s}{dx}\frac{dw_s}{dx}\right)\right] dx \quad (28)$$

Where V_e is the volume of the element; $I_1, I_2, I_3, I_4, I_5, I_6, I_7$ are the beam rigidities, defined as

$$(I_1, I_2, I_3, I_4, I_5, I_6) = b\int_{-\frac{h}{2}}^{\frac{h}{2}} E(x,z)\{1, z, f(z), zf(z), z^2, f^2(z)\}\,dz \quad (29)$$

$$I_7 = b\int_{-\frac{h}{2}}^{\frac{h}{2}} G(x,z)g^2(z)\,dz$$

The kinetic energy of the beam can be expressed as

$$T_e = \frac{1}{2}\int_{V_e} \rho_f \left(\dot{u}^2 + \dot{w}^2\right) dV \quad (30a)$$

$$T_e = \frac{1}{2} b \int_0^l \Big[J_1 \left(\dot{u}^2{}_0 + \dot{w}_b{}^2 + \dot{w}_s{}^2 + 2\dot{w}_b\dot{w}_s\right) - 2J_2\dot{u}_0\frac{d\dot{w}_b}{dx} - 2J_3\dot{u}_0\frac{d\dot{w}_s}{dx} + 2J_4\frac{d\dot{w}_b}{dx}\frac{d\dot{w}_s}{dx} + J_5\left(\frac{d\dot{w}_b}{dx}\right)^2 + J_6\left(\frac{d\dot{w}_s}{dx}\right)^2\Big] dx \quad (30b)$$

Where an over dot denotes the derivative with respect the time variable t, and the mass moments $J_1, J_2, J_3, J_4, J_5, J_6$ are defined as

$$(J_1, J_2, J_3, J_4, J_5, J_6) = b\int_{-\frac{h}{2}}^{\frac{h}{2}} \rho(x,z)\{1, z, f(z), zf(z), z^2, f^2(z)\}\,dz \quad (31)$$

B.2 Differential quadrature finite element formulation

Differential quadrature rules approximate the derivatives of a function using a weighted linear sum of field variables along a line passing through the point. For polynomial basis functions DQ, a set of Lagrange polynomials are employed as the test functions. (Cuiyun, et al., 2016).

Thus, for a field variable $f(x)$ its derivative of order n in a discrete point x_i can be expressed as:

$$\frac{\partial^n f(x;t)}{\partial x^n} = \sum_{j=1}^{N} A_{ij}^{(n)} f\left(x_j, t\right) \quad (i = 1,2,3,\ldots,N) \quad (32)$$

Where $A_{ij}^{(n)}$ is the weighting coefficient related to the derivative of order n, and the weighting coefficient is obtained as follows if $n = 1$, so

$$A_{ij}^{(1)} = \frac{M(x_i)}{(x_i - x_j)M(x_j)} \quad i \neq j, j = 1,2,\ldots,N \quad (33)$$

$$A_{ii}^{(1)} = -\sum_{j=1, j\neq i}^{n} A_{ij}^{(1)} \quad i = 1,2,\ldots,N$$

With

$$M(x_i) = \prod_{k=1, k\neq i}^{N} (x_i - x_k)$$

$$M(x_j) = \prod_{k=1, k\neq i}^{N} (x_j - x_k) \quad (34)$$

If n > 1, secondary and higher order derivatives, the weighting coefficients are determined using the following simple recurrence relationship:

$$A_{ij}^{(n)} = n\left(A_{ij}^{(1)} * A_{ii}^{(n-1)} - \frac{A_{ij}^{(n-1)}}{(x_i - x_j)}\right) \quad i \neq j, i, j = 1,2,\ldots,N, n > 1 \quad (35)$$

$$A_{ii}^{(n)} = -\sum_{j=1, j\neq i}^{N} A_{ij}^{(n)} \quad i = 1,2,\ldots,N$$

The differential quadrature finite element method was developed by (Xing and Liu, 2009), whose differential quadrature rules and Gauss-Lobatto quadrature are used to discretize the system energies. Assuming that the deflection function is

$$u(x) = \sum_{i=1}^{N} L_i(x)u_i \quad (36)$$

$$w(x) = \sum_{i=1}^{N} L_i(x)w_i$$

With L_i is the Lagrange polynomial, and $u_i = u(x_i)$, $w_i = w(x_i)$ are the displacements of the Gauss Lobatto quadrature points or the DQ nodal displacements of the beam finite element.

The matrices for the entire system are obtained according to the MEF rules for assembling elementary matrices,

$$[M]\begin{Bmatrix}\ddot{u}_0(t)\\ \ddot{w}_b(t)\\ \ddot{w}_s(t)\end{Bmatrix} + [K]\begin{Bmatrix}u_0(t)\\ w_b(t)\\ w_s(t)\end{Bmatrix} = [0] \quad (37)$$

By applying Lagrange's equations to the system discretised by the DQFEM method, we obtain the following system of differential equations:

$$[M]\{\ddot{q}\} - N_0[G]\{\mathrm{q}\} + [K]\{\mathrm{q}\} = [0] \quad (38)$$

Where:

- $[M]$and $[K]$ are respectively the total matrices after assembly matrices of mass and stiffness.
- $\{\ddot{q}\}$ and $\{\mathrm{q}\}$ are respectively the global acceleration and displacement vectors suitable for DQFEM connectivity.
- N_0 axial force which is applied through the centroid. [G] is the geometric matrix.

The programming language used is MATLAB, in order to program these solving method using the DQFEM methods.

III. RESULTS AND DISCUSSION

For buckling analysis of CNTRC beams, the present solutions based on refined higher-order beam theory

agree well with the buckling results available in the literature [8], [25] as shown in Table 3.

Table 3. Comparisons of critical loads for CNTRC beams $L/h = 10\ V_{cnt}^{*} = 0.12$

Source	UD	O
Nuttawit	0.0984	00576
Samadi	0.0986	0.0588
present	0.09845	0.05762

Table 4 compares the critical buckling loads of UD, X, O, V Beams with $\mu = \eta = 0.5$ and S_S boundary conditions and various thickness ratios L/h. As observed, as a result of changing the thickness ratios L/h=10, 15, 20 the critical buckling loads decreases with increasing the value of L/h. It is also observed that buckling loads of X-Beam are higher than V and UD-Beam. This is because X-Beam makes better use of CNT with more CNTs distributed in high bending stress regions and much less CNTs in low stress regions close to the neutral axis. Its bending stiffness, therefore, is larger than V-Beam and UD-Beam.

Table 4. Comparison of critical loads for different types of CNTRC beam for different boundary conditions with various thickness ratios L/h ($\mu = \eta = 0.5,\ f_r^{*} = 0.3$).

Type of CNT distribution	L/h		
	10	15	20
UD	0.0637	0.0287	0.0162
FG-O	0.0353	0.0157	0.0088
FG-X	0.1053	0.0484	0.0275
FG-V	0.0690	0.0311	0.0176

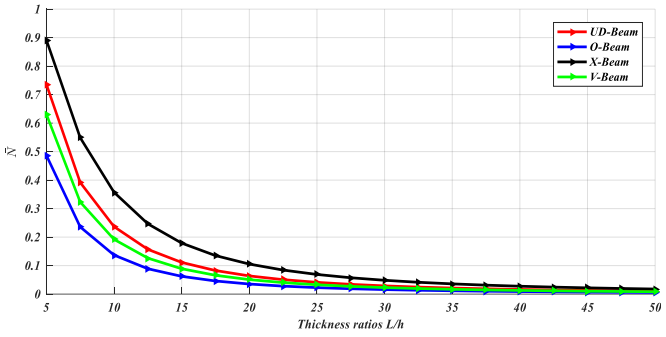

Fig. 3 Dimensionless critical buckling loads for different patterns CNTRC distribution and various thickness ratios ($\mu = \eta = 0.5, f_r^{*} = 0.3$, C-C).

Figure 3. As the length-to-thickness increases, the buckling load experiences a notable decline. The X-Beam is the strongest beam that carries the largest buckling load and followed by the UD-Beam and O-Beam.

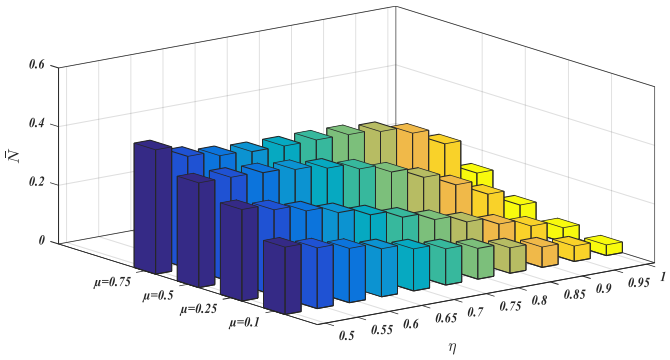

Fig. 4 Variation of critical buckling loads $\bar{N}$ beam with various thickness ratios and at various agglomeration parameters ($L/h = 10, f_r^{*} = 0.3$, C-C and X-Beam)

Figure 4 displays the 3-D bar graph variation of critical buckling loads $\bar{N}$ versus the volume ratio of the CNTs inside (η) and outside (μ) the clusters for CNT volume fraction $f_r^{*} = 0.3$ and C-C boundary condition. It can be seen that the magnitude of buckling load $\bar{N}$changes nonlinearly for variation of the (η) and (μ) and is maximum at η = 0.5 and $\mu = 0.75$ and are lowest at $= 1$, and $\mu = 0.1$.

IV. CONCLUSION

In this study the buckling analysis of CNTRC beams was investigated based on refined higher-order beam theory and by applying Lagrange's principle and DQFEM method. The beams are reinforced with various volume fraction of CNT distributions in the polymeric matrix by considering agglomeration effect of carbon nanotubes. The Eshelby-Mori-Tanaka approach are employed to model beam and estimate materials properties. The results are compared with results in the literature. The numerical results in this work led us to conclude that:

- It is found that the X-Beam is the strongest among different types of CNTRC beams in resisting buckling loads while the O-Beam is the weakest.
- The fact that mechanical properties and therefore free vibrations of CNTRC beams are seriously affected by CNTs agglomeration.
- Two parameter model of agglomeration is used to determined material properties. It is clearly shown that the agglomeration of CNTs exerts a significant weakening effect in CNT-reinforced composites. It is seen that in the case where all nanotubes are dispersed uniformly, one has μ = η, the effective Young's modulus has the maximum value

- The DQFEM method have the advantages of a simple mathematical principle, a fast convergence speed, low computation quantity, high computational accuracy and lower memory requirements, etc. According to the results obtained in this work.

REFERENCES

[1] Wan H, Delale F and Shen L, "Effect of CNT length and CNT-matrix interphase in carbon nanotube (CNT) reinforced composites," *Mech Res Commun.,* 2005, vol. 32, p. 481–489.

[2] Ajayan, P.M., Stephan, O., Colliex, C. and Trauth, D, "Aligned carbon nanotube arrays formed by cutting apolymer resin–nanotube composite", Science., 1994. vol. 256(5176), p. 1212-1214.

[3] Odegard, G.M., Gates, T.S., Wise, K.E., Park, C. and Siochi, E.J, "Constitutive modelling of nanotube-reinforced polymer composites", *Compos. Sci. Technol.,* 2003. vol. 63(11), pp. 1671-1687.

[4] Thostenson, E.T. and Chou, T.W, "On the elastic properties of carbon nanotube-based composites: Modelling and characterization", *J. Phys. A–Appl. Phys.,* 2003.vol. 36(5), p. 573-5820.

[5] Griebel, M. and Hamaekers, J, "Molecular dynamics simulations of the elastic moduli of polymer-carbon nanotube composites", *Comput. Method. Appl. Mech. Eng.,* 2004. vol. 193(17-20), p. 1773-1788.

[6] Fidelus, J.D., Wiesel, E., Gojny, F.H., Schulte, K. and Wagner, H.D, "Thermo-mechanical properties of randomly oriented carbon/epoxy nanocomposites", *Compos. Part A.,* 2005. vol. 36(11), p. 1555-1561.

[7] Hu, N., Fukunaga, H., Lu, C., Kameyama, M. and Yan, B, "Prediction of elastic properties of carbon nanotube reinforced composites", *P. Roy. Soc. A.,* 2005. vol. 461(2058), p. 1685-1710.

[8] Bakhti, K., Kaci, A., Bousahla, A.A., Houari, M.S.A., Tounsi, A. and Adda Bedia, E.A. "Large deformation analysis for functionally graded carbon nanotube-reinforced composite plates using an efficient and simple refined theory*", Steel Compos. Struct., Int. J*., 2013. vol. 14(4), p. 335-347.

[9] Barzoki, A.A.M., Loghman, A. and Arani, A.G, "Temperature-dependent nonlocal nonlinear buckling analysis of functionally graded SWCNT-reinforced microplates embedded in an orthotropic elastomeric medium", *Struct. Eng. Mech.,* 2015. vol. 53(3), p. 497-517.

[10] Bidgoli, M.R., Karimi, M.S. and Arani, A.G, "Viscous fluid induced vibration and instability of FGCNT-reinforced cylindrical shells integrated with piezoelectric layers", *Steel Compos Struct.,* 2015 vol. 19(3), p. 713-733.

[11] Ashrafi, B. and Hubert, P, "Modeling the elastic properties of carbon nanotube array/polymer composites", *Compos. Sci. Technol.,* 2006. vol. 66(3), p. 387-396.

[12] Wuite J and Adali S, "Deflection and stress behaviour of nanocomposite reinforced beams using a multiscale analysis", *Compos Struct.,* 2005. Vol. 71, p. 388–396.

[13] Vodenitcharova T and Zhang LC. , "Bending and local buckling of a nanocomposite beam reinforced by a single-walled carbon nanotube", Int J Solids Struct., 2006. vol. 43: 3006–3024.

[14] Seidel GD and Lagoudas DC, "Micromechanical analysis of the effective elastic properties of carbon nanotube reinforced composites", Mech Mater., 2006. vol. 38, p. 884–907.

[15] Qian D, Dickey EC, Andrews R, et al, "Load transfer and deformation mechanisms in carbon nanotube polystyrene composites," *Appl Phys Lett.*, 2000, Vol. 76, p. 2868–2870.

[16] Yas MH and Samadi N, " Free vibration and buckling analysis of carbon nanotube reinforced composite Timoshenko beams on elastic foundation," *Int J Pressure Vessels Piping*., 2012. vol. 98, p. 119–128.

[17] Wu C-P and Chang S-K, "Stability of carbon nanotube-reinforced composite plates with surface-bonded piezoelectric layers and under bi-axial compression," *Compos Struct*, 2014. vol. 111, p. 587–601.

[18] Barai P and Weng GJ, "A theory of plasticity for carbon nanotube reinforced composites", *Int J Plast*., 2011. vol. 27, p. 539–559.

[19] Yang Q-s, He X-q, Liu X, et al, "The effective properties and local agglomeration effect of CNT/SMP composites", *Compos Part B: Eng*., 2012, vol. 43, p. 33–38.

[20] Shokrieh M and Rafiee R, "Prediction of mechanical properties of an embedded carbon nanotube in polymer matrix based on developing an equivalent long fiber", *Mech Res Commun*., 2010. vol. 37, p. 235–240.

[21] Kamarian, S.; Shakeri, M.; Yas, M.H.; Bodaghi, M.; Pourasghar, A, "Free vibration analysis of functionally graded nanocomposite sandwich beams resting on Pasternak foundation by considering the agglomeration effect of CNTs", *J. Sandw. Struct. Mater.,* 2015. vol. 17, p. 632–665.

[22] Shi, D.-L.; Feng, X.-Q.; Huang, Y.Y.; Hwang, K.-C.; Gao, H, "The Effect of Nanotube Waviness and Agglomeration on the Elastic Property of Carbon Nanotube-Reinforced Composites", *J Eng Mater Technol*., 2004. vol. 126, p. 250–257.